Asian Journal of Control, Vol. 6, No. 2, pp. 187-198, June 2004

NANO TRAJECTORY CONTROL OF MULTILAYER LOW-VOLTAGE PZT BENDER ACTUATOR SYSTEMS

Chih-Lyang Hwang and Chau Jan

ABSTRACT

In this paper, nano trajectory control of the multilayer low-voltage PZT (lead zirconate titanate) bender actuator system (MLVPZTBAS) is developed. System analyses in of the hysteresis characteristic, frequency response and sinusoidal response, were conducted to evaluate the system features. Because not all of the states of the MLVPZTBAS are directly available, an observer is required to estimate the states. The proposed scheme contains feedback linearization with a sliding-mode controller and a state observer to estimate the system states of the MLVPZTBAS. The sliding-mode control possesses an equivalent control and a switching control. To track a trajectory dominant by a specific frequency, a reference model consisting of desired amplitude and phase features is established. The equivalent control using the signals from the observer and the reference model is designed so as to produce the desired control behavior. Due to the existence of modeling and estimation errors, the switching control is then employed to achieve robust performance. Experiments on the MLVPZTBAS were carried out to verify the usefulness of the proposed control.

KeyWords: Multilayer LVPZT bender actuator, hysteresis, observer, feedback linearization, sliding-mode control.

I. INTRODUCTION

Piezoelectric devices are commonly used when sub-micrometer displacements are desired [1-5]. Such precise displacements are needed for such purposes as machine tool design [2], biomechatronic fluid-sample-handling in DNA processing [3], optical pick-up design [4], two-degree micropositionser design [5]. There are two types of piezoelectric displacement devices that can provide this capability [6,7]. One type involves displacements about some fixed points and limited total excursion from this fixed point. The other type permits virtually unlimited displacement in the desired direction. The fixed point device is exemplified by the so-called "piezoelectric stack," in which a number of thin piezoelectric disks (usually PZT disks a few centimeters in diameter and one or two millimeters thick) are stacked on top of each other, so that mechanically, the disks are in series and electrically, they are connected in parallel [6].

If greater displacements about the fixed point are needed, there are three possible approaches. 1) The length of the stack can be increased. However, the degree of mechanical stability and robustness that can be achieved is questionable. 2) Mechanical amplification of the displacement is provided by a series of levers and amplification by a factor 20 to 30. However, the dimensions are several times larger than the length of the piezoelectric stack used in the actuator. 3) The third approach is to use bimorph (or multilayer) PZT in the form of thin piezoelectric sheets designed to blend or flex so as to produce displacements perpendicular to their thickness dimension. However, the dynamics of the bending modes must be taken into account. In this paper, the third approach is investigated (see Fig. 1). System analyses of the hysteresis characteristic, frequency response and sinusoidal response were conducted to evaluate the system. Based on these analyses, the MLVPZTBAS possesses the hysteresis characteristic, which is dependent on the polarity and magnitude of the input. To design an effective trajectory-tracking controller, the nonlinear model for the MLVPZTBAS is required.

Manuscript received February 10, 2003; revised June 10, 2003; accepted November 24, 2003.

The authors are with Department of Mechanical Engineering, Tatung University, 40 Chungshan North Road, Section 3, Taipei 10451, Taiwan.

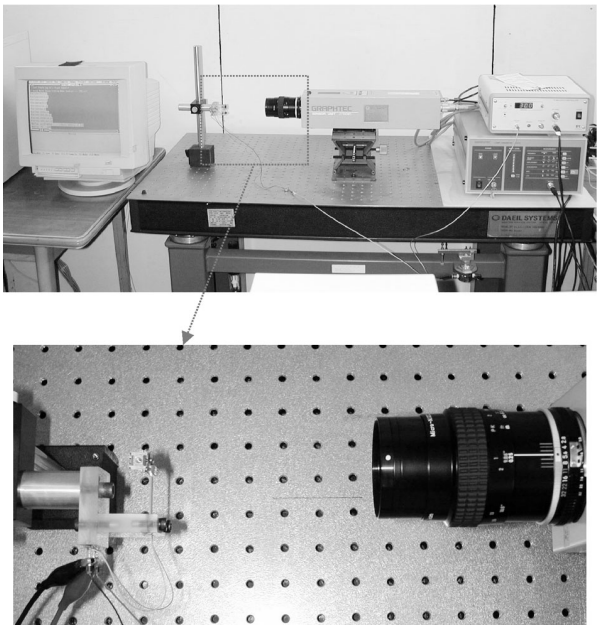

Fig. 1. The experimental setup of the MLVPZTBAS. (a) Photograph. (b) Block diagram.

Because piezoceramic materials are ferroelectric, they fundamentally exhibit hysteretic behavior in their response to an applied electric field (cf. Fig. 2). The hysteretic characteristics are generally non-differentiable nonlinearities and are usually unknown, so it is difficult to obtain an accurate trajectory tracking control [9,10]. The nonlinear dynamics of the MLVPZTBAS were identified as a modified second-order linear model coupled with a hysteresis (e.g., [11]). That paper concentrated on the control issues involved in dealing with the nonlinear hysteretic behavior displayed by most MLVPZTBASs. The paper by Ge and Jouaneh [12] compared feedforward control, PID control, and PID feedback control with hysteresis modeling in the feedforward path. The nonlinear dynamics of the MLVPZTBAS were first linearized and then reformulated into a standard almost disturbance decoupling problem [11]. However, the result was only suitable for a small operation range. The paper by Hwang *et al*., [13] proposed a forward control to approximately cancel the hysteresis and applied a discrete variable structure control to enhance performance. To suppress the vibration of a flexible beam, a spatial H_2

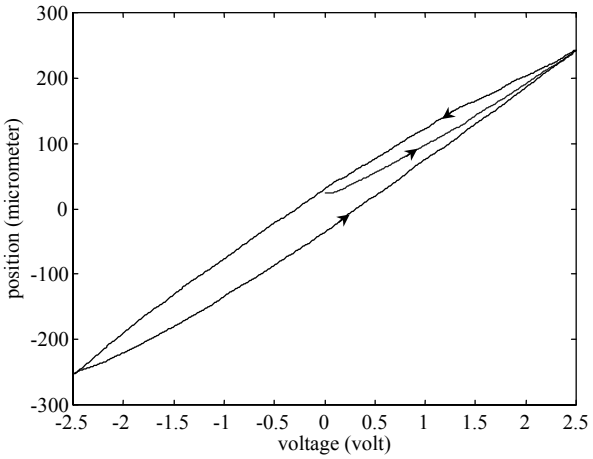

Fig. 2. Hysteresis characteristic of the MLVPZTBAS.

norm of the closed-loop system was minimized to ensure an average reduction of vibration throughout the structure [14].

It is well known that the sliding-mode control contains the following advantages: quick response, less sensitivity to uncertainties, and easy implementation [15-17]. Because not all of the states are available for the control in MLVPZTBASs, it is necessary to design an observer to estimate the system states [17]. Then, a nonlinear estimated-state-based feedback linearization controller can be applied to change the nominal system into a linear dynamic system. The proposed feedback linearization control contains a sliding-mode with an equivalent control and a switching control. To track a trajectory dominated by a specific frequency, a prescribed reference model is established to obtain a tracking error model. Then, the equivalent control based on the signals coming from the observer and the reference model is designed to produce the desired control behavior. Because piezoceramic materials are ferroelectric, they exhibit inherent nonlinearity and hysteresis. The tracking control accuracy of MLVPZTBASs may not be sufficient due to this hysteresis, the modeling error and the estimation error. Under these circumstances, the switching control was designed so as to improve the system performance.

II. EXPERIMENTAL SETUP

The experimental setup of the MLVPZTBAS consisted of five parts: a low voltage lead-zirconate-titanate bender actuator (MLVPZTBA), laser vibrometer system, power amplifier, AD/DA card interface, and control program in a personal computer (PC). A photograph and block diagram of the experimental setup are shown in Fig. 1. The specifications of the MLVPZTBA (PI–PL128.255) are given in Table 1. The MLVPZTBA offers several advantages over the classic bimorph PZTs that are manufactured by gluing two ceramic plates to-

Table 1. Properties of the MLVPZTBA.

Item \ MLVPZTBA	PI – PL128.255	Units
Operating voltage range	0 to +60	volt
Deflection	± 450	μm ± 20%
Free length	28	*mm*
Dimensions (L*W*T)	35.5*6.3*0.75	*mm*
Weight	1.2	G ± 10%
Force generation	0.5	N ± 20%

gether: fast response time and higher stiffness. The main advantage is the drastically reduced operating voltage of only 60 *volt*. The power amplifier in our setup was a single channel LVPZT controller P-862 made by the PI Co. The P-862 was used to control the output voltage from an analog input that had been connected to an analog input socket on the front panel. The nominal input was 0 ~10 *volt* for the output 0 ~100 *volt*. The feedback position of the MLVPZTBA was detected by a laser vibrometer system, models AT3500 and AT0021 from the Graphtec Co. The available measuring distance was from ±5*nm* to ±40*mm* under different conditions, the maximum sampling rate was 1.3*MHz* and the measurement resolution was 5*nm*. Different signal positions were obtained by using different input signals. The above-mentioned devices were put on a vibration isolation table (model DVIO-I Series from the Daeil Systems Co.) to reduce the effect of external disturbances. The process was repeated until the total process time finished. The time required for every process was called the "control cycle time (T_c)." In this paper, T_c = 0.0005sec.

III. SYSTEM ANALYSIS, SYSTEM MODELING AND PROBLEM FORMULATION

3.1 System analysis

The input and output relation of the proposed MLVPZTBAS, shown in Fig. 2, indicates that the hysteresis is dependent on the polarity and amplitude of the input signal (e.g., [1-13]). Subsequently, a swept sine wave with an amplitude of 0.3 *volt* and a frequency of 1~800 *Hz* was applied to the MLVPZTBAS. The corresponding input and output signals were then fed into the HP35670A to obtain the frequency response shown in Fig. 3. The results revealed that the peak occurred at about 150 *Hz*. The responses of the sinusoidal input with different amplitudes and frequencies (e.g., 2500*nm*, 30 *Hz*; 1500*nm*, 40*Hz*; and 900*nm*, 40*Hz*) are shown in Fig. 4(a), (b) and (c), respectively. The unit of position is

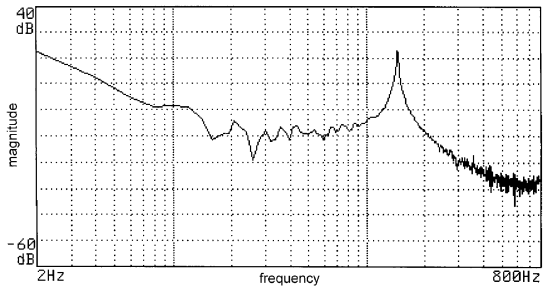

Fig. 3. Frequency response of the MLVPZTBAS.

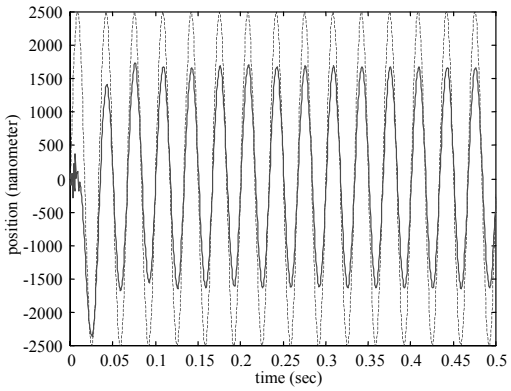

(a) $u(t) = 2500 \sin(60\pi t)nm$.

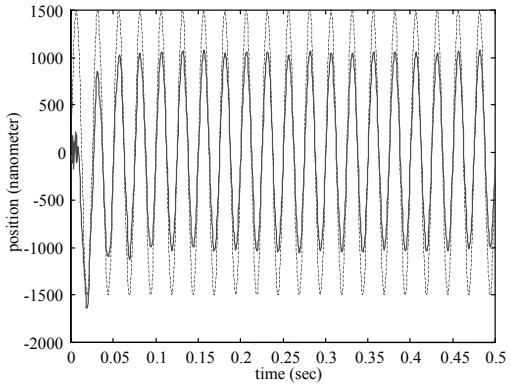

(b) $u(t) = 1500\ sin(80\pi t)nm$.

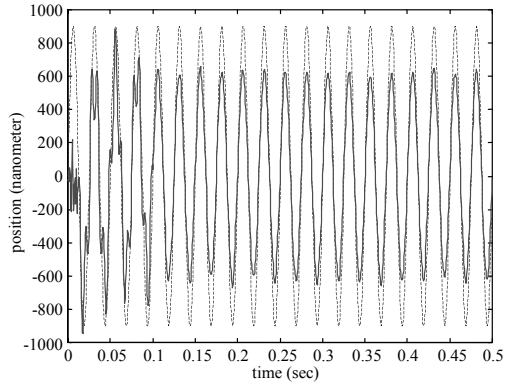

(c) $u(t) = 900 \sin(80\pi t)nm$.

Fig. 4. The sinusoidal responses of the MLVPZTBAS (–) for the sinusoidal inputs (…).

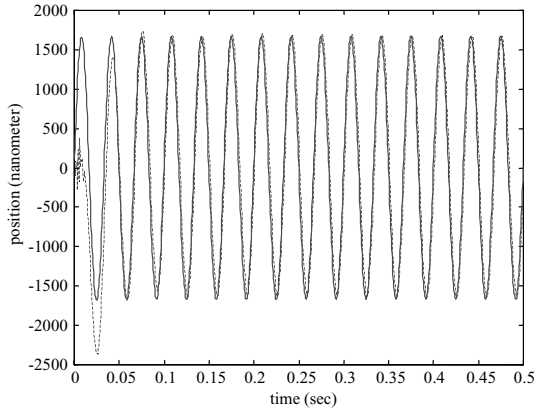

(a) $u(t) = 2500\sin(60\pi t)nm$.

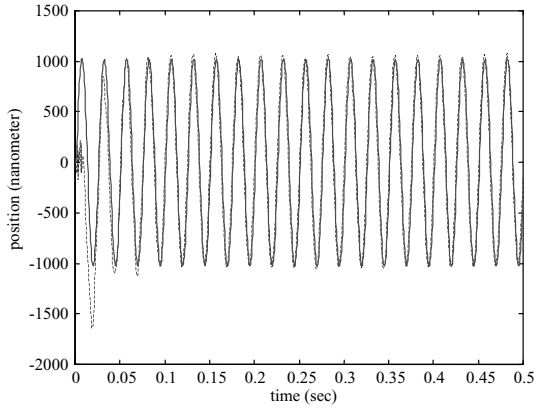

(b) $u(t) = 1500\sin(80\pi t)nm$.

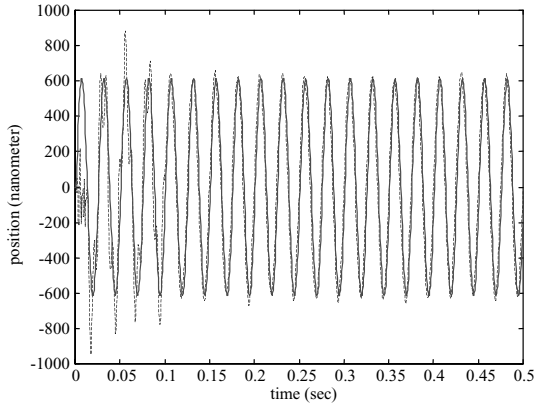

(c) $u(t) = 900\sin(80\pi t)nm$.

Fig. 5. The output responses of the nonlinear model (–) and the MLVPZTBAS (…) under different sinusoidal inputs.

micrometer, but the output signal of the laser vibrometer is voltage (unit: volt). The input signal for MLVPZTBAS is also voltage. To make a clear comparison between the input signal and the output response, the position signal with the unit "micrometer" shown in Figs. 4 and 5 was used to replace the input signal with the unit "volt". Their maximum steady-state tracking errors are presented in the first column of Table 2. In this range of the input amplitude and frequency, the effect of hysteresis was almost the same (cf. Fig. 2).

Table 2. The maximum steady-state tracking (or modeling) errors of open-loop system, nonlinear model, and MLVPZTBAS using the proposed control for six $r(t)$ or $u(t)$.

Type / $r(t)$ or $u(t)$	Open-loop system	Nonlinear model	Proposed control
2500sin(60πt) *nm* (30Hz)	920 *nm*	310 *nm*	160 *nm*
2500sin(80πt) *nm* (40Hz)	950 *nm*	315 *nm*	148 *nm*
1500sin(60πt) *nm* (30Hz)	530 *nm*	220 *nm*	115 *nm*
1500sin(80πt) *nm* (40Hz)	480 *nm*	225 *nm*	94 *nm*
900sin(60πt) *nm* (30Hz)	340 *nm*	155 *nm*	118 *nm*
900sin(80πt) *nm* (40Hz)	310 *nm*	180 *nm*	67 *nm*

3.2 System modeling

The dynamics of the MLVPZTBAS were identified as those of a second-order linear model coupled with hysteresis (see, e.g., [11]):

$$m\ddot{\varsigma}(t) + b\dot{\varsigma}(t) + \eta\varsigma(t) = \eta\left[cv(t) - h(t)\right], \tag{1a}$$

$$\dot{h}(t) = \mu\dot{v}(t) - \rho h(t) - \tau\left|\dot{v}(t)\right|h(t) - \delta\dot{v}(t)\left|h(t)\right|, \tag{1b}$$

where $\varsigma(t)$ denotes the position of the MLVPZTBAS; m, b, η and c denote the mass, damping, stiffness and effective piezoelectric coefficient, respectively; $h(t)$ stands for the output variable of the hysteretic nonlinear dynamics; $v(t)$ is the input voltage that generates an excitation force in the actuator system; and μ, τ, δ, ρ, $c > 0$ are parameters that affect the shape of the hysteresis. Because the proposed MLVPZTBAS is used for different amplitudes of trajectory tracking, the hysteretic model is dependent on the amplitude and polarity of the input signal. Define the following state:

$$\begin{aligned} x(t) &= \left[\varsigma(t) \quad \dot{\varsigma}(t) \quad h(t) \quad v(t) \quad \dot{v}(t)\right]^T \\ &= \left[x_1(t) \quad x_2(t) \quad x_3(t) \quad x_4(t) \quad x_5(t)\right]^T. \end{aligned} \tag{2}$$

Then, the system (1) can be rewritten in the following state space form:

$$\dot{x}(t) = A(x) + B\left[u(t) + d(t)\right], \tag{3a}$$

$$y(t) = C^T x(t), \tag{3b}$$

where $u(t)$ and $y(t) \in \Re$ represent the control input, and the system output, respectively; $d(t)$ denotes the bounded modeling error satisfying the matching condition; and the nominal vectors $A(x)$, B and C are described as:

$$A(x)=\begin{bmatrix} x_2(t) \\ -\left[\eta x_1(t)+bx_2(t)+\eta x_3(t)-\eta c x_4(t)\right]/m \\ \left(\mu-\delta\left|x_3(t)\right|\right)x_5(t)-\left(\rho+\tau\left|x_5(t)\right|\right)x_3(t) \\ x_5(t) \\ 0 \end{bmatrix}, \quad B=\begin{bmatrix}0\\0\\0\\0\\1\end{bmatrix}, C=\begin{bmatrix}1\\0\\0\\0\\0\end{bmatrix}. \tag{3c}$$

If $u(t) = u_m \sin(wt)$, then $x_5(t) = \dot{v}(t) = -u_m \cos(wt)/w$ and $x_4(t) = v(t) = -u_m \sin(wt)/w^2$ due to the fact that $\ddot{v}(t) = u(t)$. In summary, the sinusoidal response of the nonlinear model (1) is achieved by using the above-mentioned relation. Based on model verification performed using the sinusoidal response of the nonlinear model (1) and the MLVPZTBAS (cf. Fig. 5), the coefficients of the MLVPZTBAS were found to be as follows: $m = 0.016kg$, $b = 1.2 \times 10^{-6} Ns/\mu m$, $\eta = 5 \times 10^{-4} N/\mu m$, $c = 3050 \mu m/V$, $\mu = 0.48$, $\rho = 0.2 s^{-1}$, $\tau = 0.2(\mu m)^{-1}$ and $\delta = 0.3(\mu m)^{-1}$. In addition, the maximum modeling errors are shown in the second column of Table 2. Based on Table 2, the relative maximum tracking error for different amplitudes and frequencies ranges from 12% to 20%. Thus, the proposed model under the desired range of amplitude and frequency is accurate enough. The system (3) has a relative degree of four.

3.3 Problem formulation

Because only the laser vibrometer system is applied to measure the dynamic position, the states of the system (1) must be estimated. The following nonlinear observer is employed to estimate the states (e.g., [17]):

$$\dot{\hat{x}}(t) = A(\hat{x}) + Bu(t) + L(y(t) - \hat{y}(t)), \tag{4a}$$

$$\hat{y}(t) = C^T \hat{x}(t), \tag{4b}$$

where

$$\hat{x}(t) = \left[\hat{\varsigma}(t) \quad \dot{\hat{\varsigma}}(t) \quad \hat{h}(t) \quad \hat{v}(t) \quad \dot{\hat{v}}(t)\right]^T = \left[\hat{x}_1(t) \quad \hat{x}_2(t) \quad \hat{x}_3(t) \quad \hat{x}_4(t) \quad \hat{x}_5(t)\right]^T$$

denotes the estimated state; the vectors $A(\hat{x})$, B and C are the same functions as in (3) except for the arguments; L denotes the observer gain; and $u(t)$ and $\hat{y}(t) \in \Re$ represent the output of the controller and the nonlinear observer, respectively. After the states are estimated, coordinate transformation is applied to design a feedback linearizing control (e.g., alluded to in [18]). To track a trajectory dominated by a specific frequency, a prescribed reference model is also employed to obtain a tracking error model. To enhance the system performance, the design of the sliding-mode in the feedback linearizing control is considered. The sliding-mode control contains two parts: one is an equivalent control, and the other is a switching control. The equivalent control based on the signals coming from the observer and the reference model is constructed so as to produce the desired control behavior. Because the piezoceramic materials are ferroelectric, they have inherent hysteretic nonlinearity that is not a one-to-one mapping and is dependent on the polarity of the input signal; i.e., the modeling error $d(t)$ in (1) occurs. In addition, the estimation error cause the system performance to deteriorate. Under these circumstances, the switching control is designed so as to improve the system performance (alluded to in Fig. 6).

IV. FEEDBACK LINEARIZING CONTROL

The following lemma is used to discuss the transformation of the system (3) into the "normal form." This form decomposes the system into an external part Ψ and an internal part Φ. The external part is linearized by the state feedback control. The internal part is made unobservable by the same control [19].

Lemma 1 [18,19]. Consider the nonlinear system (3) with the following global diffeomorphism: $z(t) = T(x) = [\Psi^T(x) \ \Phi^T(x)]^T$ where $[\partial\Psi(x)/\partial x(t)]A(x) = A_c\Psi(x) - B_c\beta^{-1}(x)\alpha(x)$ and $[\partial\Phi(x)/\partial x]B = 0$. Then the following dynamic system is achieved:

$$\dot{\Psi}(x) = A_c\Psi(x) + B_c\beta_0^{-1}(\Psi,\Phi)[u(t) - \alpha_0(\Psi,\Phi) + d(t)], \tag{5a}$$

$$\dot{\Phi}(x) = A_0(\Psi,\Phi), \tag{5b}$$

where $\Psi(x) \in \Re^4$ and $\Phi(x) \in \Re$. Moreover, the functions $\alpha_0(\Psi, \Phi)$ and $\beta_0(\Psi, \Phi)$ are the functions $\alpha(x) = -\{[\partial\psi_4(x)/\partial x]A(x)\}/\{[\partial\psi_4(x)/\partial x]B\}$ and $\beta(x) = 1/\{[\partial\psi_4(x)/\partial x]B\}$ at $x(t) = T^{-1}(z)$, respectively. $A_0(\Psi, \Phi)$ is the representation in the transformed coordinate $x(t) = T^{-1}(z)$ of $[\partial\Phi(x)/\partial x]A(x)$. The matrices A_c, B_c are described as follows:

$$A_c=\begin{bmatrix}0&1&0&0\\0&0&1&0\\0&0&0&1\\0&0&0&0\end{bmatrix}, \quad B_c=\begin{bmatrix}0\\0\\0\\1\end{bmatrix}. \tag{6}$$

Setting $\Psi(x) = 0$ in (5b) results in $\dot{\Phi}(x) = A_0(0, \Phi)$, which is called the "zero dynamics". The system is said to be minimum phase if $\dot{\Phi}(x) = A_0(0, \Phi)$ has an as-

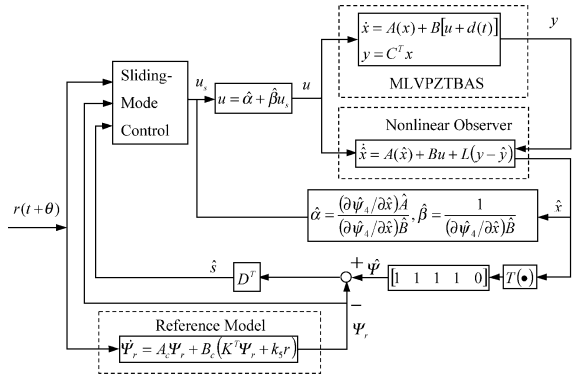

Fig. 6. Control block diagram.

ymptotically stable equilibrium point in the domain of interest. Thus, the coordinate transformation performed using the estimation state $\hat{x}(t)$ is defined as follows: $\hat{z}(t) = T(\hat{x}) = [\Psi^T(\hat{x})\ \ \Phi^T(\hat{x})]^T$. Then the estimated dynamic system in the $z(t)$-coordinate is obtained from the nominal system (3) for the design of the feedback linearizing control:

$$\dot{\hat{\Psi}}(t) = A_c\hat{\Psi}(t) + B_c\beta_0^{-1}(\hat{\Psi},\hat{\Phi})[u(t) - \alpha_0(\hat{\Psi},\hat{\Phi})], \tag{7a}$$

$$\dot{\hat{\Phi}}(t) = A_0(\hat{\Psi},\hat{\Phi}), \tag{7b}$$

where $\hat{\Psi}(t) = \Psi(\hat{x}) \in \Re^4$ and $\hat{\Phi}(t) = \Phi(\hat{x}) \in \Re$. In addition, the functions $\alpha_0(\hat{\Psi},\hat{\Phi})$ and $\beta_0(\hat{\Psi},\hat{\Phi})$ are the functions

$$\alpha(\hat{x}) = -\{[\partial\psi_4(\hat{x})/\partial\hat{x}]A(\hat{x})\}/\{[\partial\psi_4(\hat{x})/\partial\hat{x}]B\}$$

and $\beta(\hat{x}) = 1/\{[\partial\psi_4(\hat{x})/\partial\hat{x}]B\}$ at $\hat{x}(t) = T^{-1}(\hat{z})$, respectively. $A_0(\hat{\Psi},\hat{\Phi})$ is the representation in the transformed coordinate $\hat{x}(t) = T^{-1}(\hat{z})$ of $[\partial\Phi(\hat{x})/\partial\hat{x}]A(\hat{x})$. In the following, the symbol $\hat{\alpha}(t) = \alpha(\hat{x})$ is used alternatively.

The following reference model with the desired amplitude and phase features (8) is designed to track a trajectory dominated by a specific frequency, e.g., sinusoidal trajectory:

$$\begin{aligned} \dot{\Psi}_r(t) &= A_c\Psi_r(t) + B_c\{K^T\Psi_r(t) + k_5 r(t+\theta)\}, \\ y_r(t) &= C_c^T\Psi_r(t), \end{aligned} \tag{8}$$

where $y_r(t)$ denotes the output of the reference model, $C_c^T = [1\ \ 0\ \ 0\ \ 0]$, and $K^T = [k_1\ \ k_2\ \ k_3\ \ k_4] \in \Re^4$ is selected such that the desired response is obtained. According to the sinusoidal trajectory $A_m\sin(wt)$ the values of k_1, k_2, k_3, k_4, k_5 and θ are chosen such that $|H(jw)| = |C_c^T(jwI - A_c - B_cK^T)^{-1}B_ck_5| = 1$ and $\angle H(jw) = \theta$. For example, if the values of k_1, k_2, k_3 and k_4 are chosen first, then

$$k_5 = \sqrt{(w^4 - k_3w^2 + k_1)^2 + (-k_4w^3 + k_2w)^2}$$

and

$$\theta = -\tan^{-1}[-k_4w^3 + k_2w/w^4 - k_3w^2 + k_1]$$

are assigned.

The state tracking error model of the system (5) can be written as follows:

$$\begin{aligned} \dot{\Psi}_e(t) = A_c\Psi_e(t) + B_c\{&\beta_0^{-1}(\Psi,\Phi)[u(t) \\ &-\alpha_0(\Psi,\Phi) + d(t)] - K^T\Psi_r(t) - k_5 r(t)\}, \end{aligned} \tag{9}$$

where $\Psi_e(t) = \Psi(x) - \Psi_r(t)$ represents the state tracking error. Based on the nonlinear observer and its feedback linearization, the proposed controller is as follows:

$$\begin{aligned} u(t) &= \alpha_0(\hat{\Psi},\hat{\Phi}) + \beta_0(\hat{\Psi},\hat{\Phi})u_s(t) \\ &= \alpha_0(\Psi,\Phi) + \beta_0(\Psi,\Phi)u_s(t) \\ &\quad + [\alpha_0(\hat{\Psi},\hat{\Phi}) - \alpha_0(\Psi,\Phi)] \\ &\quad + [\beta_0(\hat{\Psi},\hat{\Phi}) - \beta_0(\Psi,\Phi)]u_s(t), \end{aligned} \tag{10}$$

where $u_s(t)$ is a sliding-mode control discussed in the next section. In summary, the feedback linearizing control $u(t)$ in (10) contains a sliding-mode $u_s(t)$ that is employed to improve the system performance.

V. SLIDING-MODE CONTROL

Sliding-mode control is a powerful approach to the control of nonlinear and uncertain dynamic systems [15-17]. A sliding surface is first defined as follows:

$$s(t) = D^T\Psi_e(t), \tag{11}$$

where

$$\begin{aligned} \Psi_e(t) &= [\psi_{e1}(t)\ \ \psi_{e2}(t)\ \ \psi_{e3}(t)\ \ \psi_{e4}(t)]^T \\ &= [\psi_{e1}(t)\ \ \dot{\psi}_{e1}(t)\ \ \ddot{\psi}_{e1}(t)\ \ \dddot{\psi}_{e1}(t)]^T \end{aligned}$$

and $D = [d_4\ \ d_3\ \ d_2\ \ d_1]^T$. The coefficients d_i, i = 1, 2, 3, 4 are chosen so that the sliding surface $s(t)$ = 0 is stable.

Let $\tilde{\Psi}(t) = \Psi(x) - \hat{\Psi}(t)$ and $\bar{\Psi}(t) = \hat{\Psi}(t) - \Psi_r(t)$, where $\tilde{\Psi}(t)$ and $\bar{\Psi}(t)$ denote the state estimation error and the estimation tracking error in the $z(t)$-coordinate, respectively. From (11), the estimated sliding surface is defined as follows:

$$\hat{s}(t) = D^T\bar{\Psi}(t) = s(t) - D^T\tilde{\Psi}(t) \tag{12}$$

where $\bar{\Psi}(t) = [\bar{\psi}_1(t)\ \ \bar{\psi}_2(t)\ \ \bar{\psi}_3(t)\ \ \bar{\psi}_4(t)]^T$. That is, the estimation of the sliding surface, $\hat{s}(t)$, is the linear

combination of the estimation tracking error in the $z(t)$-coordinate; it is also equal to the original sliding surface, $s(t)$ minus the estimation error of the sliding surface, $D^T\tilde{\Psi}(t)$.

From (12) and the triangular inequality, equation (13) is obtained:

$$|\hat{s}(t)|+|D^T\tilde{\Psi}(t)|\geq|s(t)| \quad \text{or} \quad |s(t)|+|D^T\tilde{\Psi}(t)|\geq|\hat{s}(t)|. \tag{13}$$

The system (2) can be rewritten in the following form:

$$\dot{x}(t)=A_l x(t)+A_n(x)+B[u(t)+d(t)], \tag{14}$$

where

$$A_l=\begin{bmatrix} 0 & 1 & 0 & 0 & 0 \\ -\eta/m & -b/m & -\eta/m & \eta c/m & 0 \\ 0 & \mu & -\rho & 0 & 0 \\ 0 & 0 & 0 & 0 & 1 \\ 0 & 0 & 0 & 0 & 0 \end{bmatrix}, \tag{15}$$

$$A_n(x)=\begin{bmatrix} 0 \\ 0 \\ -\delta\ |x_3(t)|x_5(t)-\tau|x_5(t)|x_3(t) \\ 0 \\ 0 \end{bmatrix}. \tag{16}$$

Similarly, the nonlinear observer (4) can be rewritten in the following form:

$$\dot{\hat{x}}(t)=A_l\hat{x}(t)+A_n(\hat{x})+Bu(t)+L(y(t)-\hat{y}(t)). \tag{17}$$

Taking the time derivative of $\tilde{x}(t)$ gives

$$\begin{aligned}\dot{\tilde{x}}(t)&=(A_l-LC)\tilde{x}(t)+\Delta A_n(t)+Bd(t)\\&=A_L\tilde{x}(t)+\Delta A_n(t)+Bd(t),\end{aligned} \tag{18}$$

where $\tilde{x}(t)=x(t)-\hat{x}(t)$ denotes the state estimation error in the $x(t)$-coordinate:

$$\Delta A_n(t)=A_n(x)-A_n(\hat{x}), \tag{19}$$

$$A_L=A_l-LC. \tag{20}$$

Lemma 2. Since (A_l, C) is observable, the matrix A_L is Hurwitz for a suitable choice of the observer gain L. There exist, therefore, symmetric and positive-definite matrices P and Q which satisfy

$$A_L^TP+PA_L=-Q. \tag{21}$$

The symbols $Q_m=\min\{\lambda(Q)\}$, $Q_M=\max\{\lambda(Q)\}$ and $\|Q\|^2=\max\{\lambda(Q^TQ)\}$ are also used here. It can be verified from (19) and (16) that $A_n(x)$ is locally Lipschitz; thus, there exists a positive constant ξ_1 such that

$$\|A_n(x)-A_n(\hat{x})\|\leq\xi_1\|x(t)-\hat{x}(t)\|, \tag{22}$$

where $\|\cdot\|$ denotes the usual Euclidean norm. Similarly, there exists a positive constant ξ_2 yielding

$$\|\Psi(x)-\Psi(\hat{x})\|\leq\xi_2\|x(t)-\hat{x}(t)\|.. \tag{23}$$

Lemma 3. There exists a positive constant δ_1 such that the following inequality for the modeling error $d(t)$ is obtained:

$$\|d(t)\|\leq\delta_1. \tag{24}$$

The proposed sliding-mode control is designed as follows:

$$u_s(t)=u_{eq}(t)+u_{sw}(t), \tag{25}$$

where

$$u_{eq}(t)=D^TA_c[\hat{\Psi}(t)-\Psi_r(t)]+K^T\Psi_r(t)+k_5r(t+\theta), \tag{26}$$

$$\begin{aligned}&u_{sw}(t)=-[\gamma_1\hat{s}(t)+\gamma_2\hat{s}(t)/|\hat{s}(t)|]/(1-\gamma_0),\\&\gamma_1,\gamma_2>0,\ 1>\gamma_0\geq0.\end{aligned} \tag{27}$$

Before launching into the main theorem of this paper, the derivative of the sliding surface is given as follows. Using (11), (9), (10), (25) and (26) yields

$$\begin{aligned}\dot{s}(t)&=D^T\dot{\Psi}_e(t)\\&=D^T\{A_c\Psi_e(t)+B_c[\beta_0^{-1}(\Psi,\Phi)(u(t)-\alpha_0(\Psi,\Phi)\\&\quad+d(t))-K^T\Psi_r(t)-k_5r(t+\theta)]\}\\&=D^T\{A_c\Psi_e(t)+B_c[u_s(t)+\beta_0^{-1}(\Psi,\Phi)(\alpha_0(\hat{\Psi},\hat{\Phi})\\&\quad-\alpha_0(\Psi,\Phi))+\beta_0^{-1}(\Psi,\Phi)(\beta_0(\hat{\Psi},\hat{\Phi})\\&\quad-\beta_0(\Psi,\Phi))u_s(t)-K^T\Psi_r(t)-k_5r(t+\theta)\\&\quad+\beta_0^{-1}(\Psi,\Phi)d(t)]\}\\&=D^T\{A_c\tilde{\Psi}(t)+\beta_0^{-1}(\Psi,\Phi)d(t)\\&\quad+B_c[u_{sw}(t)+\beta_0^{-1}(\Psi,\Phi)(\alpha_0(\tilde{\Psi},\tilde{\Phi})\\&\quad+\beta_0(\tilde{\Psi},\tilde{\Phi})(u_{eq}(t)+u_{sw}(t)))]\}\\&=[1+\beta_0^{-1}(\Psi,\Phi)\beta_0(\tilde{\Psi},\tilde{\Phi})]u_{sw}(t)+F_1(t),\end{aligned} \tag{28}$$

where

$$\alpha_0(\tilde{\Psi},\tilde{\Phi})=\alpha_0(\hat{\Psi},\hat{\Phi})-\alpha_0(\Psi,\Phi)=\tilde{\alpha}_0(t),$$

$$\beta_0(\tilde{\Psi},\tilde{\Phi})=\beta_0(\hat{\Psi},\hat{\Phi})-\beta_0(\Psi,\Phi)=\tilde{\beta}_0(t),$$

and

$$F_1(t) = D^T A_c \tilde{\Psi}(t) + D^T \beta_0^{-1}(\Psi,\Phi) d(t) + \beta_0^{-1}(\Psi,\Phi)\alpha_0(\tilde{\Psi},\tilde{\Phi}) + \beta_0^{-1}(\Psi,\Phi)\beta_0(\tilde{\Psi},\tilde{\Phi}) u_{eq}(t).$$

Then the multiplication of $s(t)\dot{s}(t)$ is simplified by using (28), (12) and (27):

$$\begin{aligned} s(t)\dot{s}(t) &= [\hat{s}(t) + D^T\tilde{\Psi}(t)] \\ &\quad \cdot \{[1+\beta_0^{-1}(\Psi,\Phi)\beta_0(\tilde{\Psi},\tilde{\Phi})]u_{sw}(t) + F_1(t)\} \\ &= -[1+\beta_0^{-1}(\Psi,\Phi)\beta_0(\tilde{\Psi},\tilde{\Phi})] \\ &\quad \cdot [\gamma_1 \hat{s}^2(t) + \gamma_2 |\hat{s}(t)|]/(1-\gamma_0) \\ &\quad + D^T\tilde{\Psi}(t)\{[1+\beta_0^{-1}(\Psi,\Phi)\beta_0(\tilde{\Psi},\tilde{\Phi})]u_{sw}(t) \\ &\quad + F_1(t)\} + \hat{s}(t)F_1(t) \\ &\le -\{\gamma_1[(s(t)-D^T\tilde{\Psi}(t))(s(t)-D^T\tilde{\Psi}(t))] \\ &\quad + \gamma_2 |\hat{s}(t)|\} \\ &\quad + D^T\tilde{\Psi}(t)\{[1+\beta_0^{-1}(\Psi,\Phi)\beta_0(\tilde{\Psi},\tilde{\Phi})]u_{sw}(t) \\ &\quad + F_1(t)\} + \hat{s}(t)F_1(t) \\ &= -\{\gamma_1 s^2(t) + \gamma_2 |\hat{s}(t)| + \gamma_1 \tilde{\Psi}^T(t) D^T D \tilde{\Psi}(t)\} \\ &\quad + F_2(t) \\ &\le -\{\gamma_1 s^2(t) + \gamma_2 |\hat{s}(t)|\} + F_2(t), \end{aligned} \tag{29}$$

where

$$\begin{aligned} F_2(t) &= 2\gamma_1 s(t) D^T\tilde{\Psi}(t) + D^T\tilde{\Psi}(t) \\ &\quad \cdot \{[1+\beta_0^{-1}(\Psi,\Phi)\beta_0(\tilde{\Psi},\tilde{\Phi})]u_{sw}(t) \\ &\quad + F_1(t)\} + \hat{s}(t)F_1(t), \end{aligned} \tag{30}$$

and the first inequality has used the following assumption:

$$\left|\beta_0^{-1}(\Psi,\Phi)\beta_0(\tilde{\Psi},\tilde{\Phi})\right| < \gamma_0 < 1. \tag{31}$$

Lemma 4. The lemma gives the upper bound of the uncertainties $F_2(t)$:

$$\begin{aligned} |F_2(t)| &\le c_1 |s(t)|^2 + c_2 |s(t)| \|\tilde{x}(t)\| + c_3 \|\tilde{x}(t)\| \\ &\quad + c_4 |s(t)| + c_5 \|\tilde{x}(t)\|^2, \end{aligned} \tag{32}$$

where c_1, c_2, c_3, c_4 and c_5 are constants.

The values of γ_2 in (27) are chosen and are sufficiently large such that

$$-\gamma_2 |\hat{s}(t)| + (c_3 + 2\delta_1 \|PB\|)\|\tilde{x}(t)\| + c_4 |s(t)| < 0. \tag{33}$$

Then, the following result can be obtained from (13), (23) and (33).

$$\begin{aligned} \gamma_2 &> [(c_3 + 2\delta_1\|PB\|)\|\tilde{x}(t)\| + c_4|s(t)|]/|\hat{s}(t)| \\ &> [(c_3 + 2\delta_1\|PB\|)\|\tilde{x}(t)\| + c_4|s(t)|]/[\xi_2 |D^T\tilde{x}(t)| + |s(t)|]. \end{aligned} \tag{34}$$

As $|s(t)| >> \xi_2 |D^T\tilde{x}(t)|$, $\gamma_2 > c_4$ is selected. Similarly, as $s(t) << \xi_2 |D^T\tilde{x}(t)|$, $\gamma_2 > (c_3 + 2\delta_1\|PB\|)/(\xi_2\|D\|)$ is chosen. As

$$O(|s(t)|) = O(\xi_2 |D^T\tilde{x}(t)|) = \upsilon \text{ or } O(|\hat{s}(t)|) = \upsilon$$

(where $O(\cdot)$ denotes the order of the corresponding argument, and $\upsilon < 0$), γ_2 becomes very large; however, the operating point is in the neighborhood of the sliding surface. Hence, the inequality (33) or (34) is satisfied by a suitable selection of γ_2, e.g.,

$$\gamma_2 = \max\{c_4, (c_3 + 2\delta_1\|PB\|)/(\xi_2\|D\|)\},$$

as the operating point is not in the neighborhood of

$$O(|s(t)|) = O(\xi_2 |D^T\tilde{x}(t)|) = \upsilon \text{ or } O(|\hat{s}(t)|) = \upsilon.$$

Definition 2 [18]. The solutions of a dynamic system are said to be uniformly ultimately bound (UUB) if there exist positive constants υ and κ, and if for every $\Delta \in (0, \kappa)$, there is a positive constant $T = T(\Delta)$ such that $\|x(t_0)\| < \Delta \Rightarrow \|x(t)\| \le \upsilon$, $\forall t \ge t_0 + T$.

The main theorem of the paper is given below:

Theorem 1. Consider the closed-loop system, including the state tracking error system (9), the nonlinear observer (4), and the sliding-mode controller (25)-(27). The overall system satisfies the following conditions: (i) assumption (31); (ii) the selection of a switching gain γ_2 satisfying (34) and $\gamma_1 > \varepsilon/2 + c_1$, where $\varepsilon > 0$; (iii) $|\Gamma| > 0$, where

$$\Gamma = \begin{bmatrix} \gamma_1 - \varepsilon/2 - c_1 & c_2/2 \\ c_2/2 & Q_m - 2\xi_1 P_M - \varepsilon P_M - c_5 \end{bmatrix}. \tag{35}$$

Then, $\{s(t), \hat{s}(t), u(t), u_s(t), x(t), \hat{x}(t), \Psi(t), \hat{\Psi}(t)\}$ are UUB, and the system performance exponentially converges to the following region:

$$\{(s,\tilde{x},\hat{s}) | O(|s(t)|) = O(\xi_2 |D^T\tilde{x}(t)|) = \upsilon \text{ or } O(\hat{s}(t)) = \upsilon\}. \tag{36}$$

Proof. See the Appendix.

Remark 1. If the control input is not smooth, the switching control can be modified as follows:

$$u_{sw}(t) = -[\gamma_1 \hat{s}(t) + \gamma_2 \hat{s}(t) / (|\hat{s}(t)| + \bar{\varepsilon})] / (1 - \gamma_0), \ \bar{\varepsilon} \geq 0. \quad (37)$$

Remark 2. The procedure for designing the controller is summarized as follows:

Step 1. The nominal nonlinear model (2) is employed to capture the dynamics of the MLVPZTBAS.
Step 2. A nonlinear state feedback linearization controller (10) is applied to change the system into a linear dynamic system.
Step 3. Because the states (i.e., $x_2(t)$, $x_3(t)$, $x_4(t)$ and $x_5(t)$) of the MLVPZTBAS model are not accessible, a nonlinear observer (4) is employed to estimate the states (i.e., $\hat{x}_2(t)$, $\hat{x}_3(t)$, $\hat{x}_4(t)$ and $\hat{x}_5(t)$).
Step 4. To track a trajectory dominated by a specific frequency, the reference model (8) is established.
Step 5. Based on the observer and the reference model, the equivalent control (26) is designed.
Step 6. Due to the existence of uncertainties, the control performance of the MLVPZTBAS is generally poor. The switching control (27) is then employed to improve the performance.
Step 7. Finally, the proposed controller (10), (25) for the MLVPZTBAS is obtained (cf. Fig. 6).

VI. EXPERIMENTAL RESULTS

The coefficients of the reference model were selected as follows: $K^T = [-2000 \ \ -400 \ \ -170 \ \ -18]$; i.e., the corresponding poles were –0.5591±3.7872*i*, –8.4409±8.0758*i*. The coefficients of the sliding surface (11) were selected as $D^T = [200 \ \ 90 \ \ 10 \ \ 1]$; i.e., the corresponding poles were –3.5613±7.5381*i* and –2.8775. The control parameters $\gamma_1 = 30$, $\gamma_2 = 10$ and $\gamma_0 = 0.1$ for the switching control $u_{sw}(t)$ were chosen. To obtain the Hurwitz matrix $(A_l - L_C)$ in (20), the observer gain L was chosen as $L = [2.5 \ \ 10 \ \ 10 \ \ 5 \ \ 5]^T$, and the eigenvalues of the observer were –82±94*i*, –7.5, –5 and –5. The coordinate transformation produced the following result:

$$\begin{aligned} &\psi_1(\hat{x}) = \hat{x}_1(t), \psi_2(\hat{x}) = A_1(\hat{x}), \psi_3(\hat{x}) = A_2(\hat{x}), \\ &\psi_4(\hat{x}) = -[\eta A_1(\hat{x}) + bA_2(\hat{x}) + \eta A_3(\hat{x}) - \eta c A_4(\hat{x})] / m, \\ &\Phi(\hat{x}) = \hat{x}_4(t), \end{aligned} \quad (38)$$

where $A_i(\hat{x})$ denotes the *ith* component of $A(\hat{x})$ Then, $\dot{\Phi}(\hat{x}) \leq -\xi \Phi(\hat{x})$, where $\xi = \rho / (1 - \mu / c) > 0$, was exponentially stable because $c > \mu > 0$. Furthermore, $\partial T(\hat{x}) / \partial \hat{x}$ was nonsingular for all $\dot{x}(t)$.

The output responses of the proposed control for the reference inputs $2500\sin(60\pi t)nm$, $1500\sin(80\pi t)nm$ and $900\sin(80\pi t)nm$ are presented in Fig. 7(a), (b) and (c), respectively. The maximum steady-state tracking errors with respect to the corresponding amplitudes of the reference input were 6.4%, 6.2% and 7.4%, respectively (cf. Table 2). These tracking results are accurate enough. In addition, the corresponding control inputs are all smooth enough. For the sake of brevity, only the control input of the reference input $900\sin(80\pi t)nm$ case is shown in Fig. 8. Similarly, Fig. 9 depicts the tracking error of the proposed control for the reference input $900\sin(80\pi t)nm$ Based on the above-mentioned results, it can be seen that the proposed control is suitable for the nano-trajectory tracking of MLVPZTBASs.

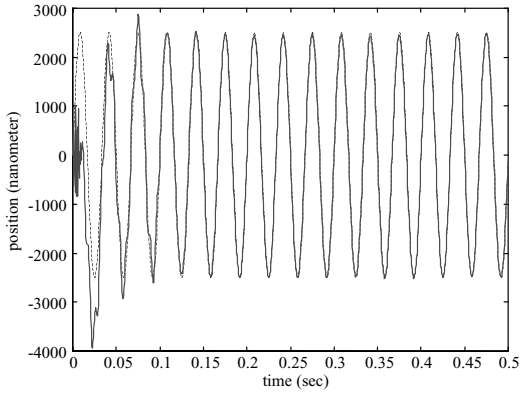

(a) $r(t) = 2500 \sin(60\pi t)nm$

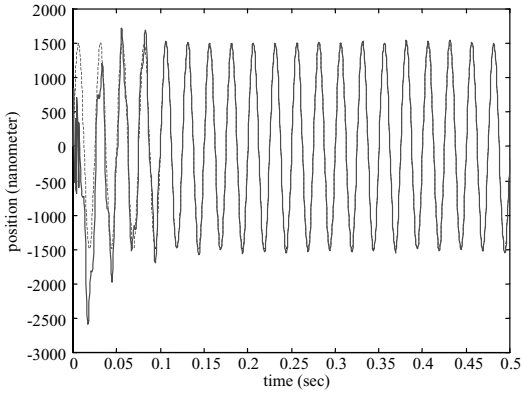

(b) $r(t) = 1500 \sin(80\pi t)nm$

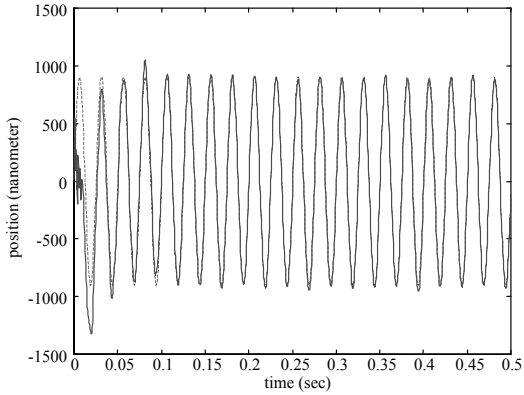

(c) $r(t) = 900 \sin(80\pi t)nm$

Fig. 7. The output responses of the proposed control (–) under different reference inputs (…).

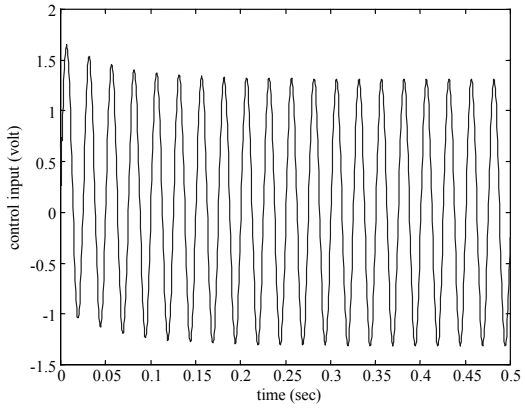

Fig. 8. The control input of the proposed control for the reference input $r(t) = 900 \sin(80\pi t)nm$.

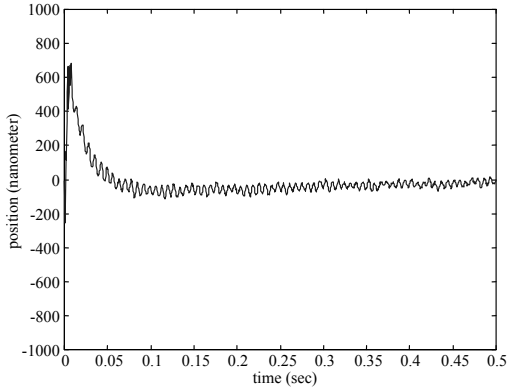

Fig. 9. The tracking error of the proposed control for the reference input $r(t) = 900 \sin(80\pi t)nm$.

VII. CONCLUSIONS

Because piezoceramic materials are ferroelectric, they fundamentally exhibit hysteretic behavior in their response to an applied electric field. There are two difficulties involved in modeling such hysteretic nonlinearity. Firstly, it exhibits non-local memory. Secondly, the nonlinear hysteresis loop displays asymmetry. The most important part of the MLVPZTBAS is the piezoelectric actuator, and there is usually only a position sensor inside it. The proposed control scheme offers effective tracking control of MLVPZTBASs whose system states are unavailable. The uncertainties in the proposed control system include the modeling error of the MLVPZTBAS, the estimation error of the state, and the external disturbance. Under these uncertain conditions, the switching control is applied to enhance the robust performance. The parameters γ_1 and γ_2 in the switching control are chosen, and they must be large enough to cope with these uncertainties. However, if the values of these parameters are too large, the result may be chattering control input. In this situation, a better but less complex modeling of the MLVPZTBAS is suggested.

APPENDIX

For the sake of brevity, the arguments for the signals are omitted if it does not lead to confusion. Define a Lyapunov function candidate for the closed-loop system as follows:

$$V = s^2/2 + \tilde{x}^T P \tilde{x} > 0, \text{ as } s \neq 0, \tilde{x} \neq 0. \tag{A1}$$

Let $\dot{\bar{V}} = \dot{V} + \varepsilon V$, where $\varepsilon > 0$. The time derivative of $\bar{V}$ is given by

$$\dot{\bar{V}} = s\dot{s} + \dot{\tilde{x}}^T P\tilde{x} + \tilde{x}^T P\dot{\tilde{x}} + \varepsilon(s^2/2 + \tilde{x}^T P\tilde{x}). \tag{A2}$$

Substituting (29) into (A2) yields

$$\begin{aligned}\dot{\bar{V}} = &-[\gamma_1 s^2 + \gamma_2 |\hat{s}|] + F_2 + \varepsilon s^2/2 + \dot{\tilde{x}}^T p\tilde{x} \\ &+ \tilde{x}^T P\dot{\tilde{x}} + \tilde{x}^T \varepsilon P\tilde{x}.\end{aligned} \tag{A3}$$

Substituting (18) and (22) into (A3), the time derivative of $\bar{V}$ is given by

$$\begin{aligned}\dot{\bar{V}} = &-[\gamma_1 s^2 + \gamma_2 |\hat{s}|] + F_2 + \varepsilon s^2/2 - \tilde{x}^T Q\tilde{x} + \Delta A_n^T P\tilde{x} \\ &+ \tilde{x}^T P\Delta A_n + (Bd)^T P\tilde{x} + \tilde{x}^T PBd + \tilde{x}^T \varepsilon P\tilde{x}.\end{aligned} \tag{A4}$$

Taking the norm of (A4) by using the relations (22), (23), (24) and (32) gives

$$\begin{aligned}\dot{\bar{V}} &\leq -[\gamma_1 |s|^2 + \gamma_2 |\hat{s}| + |F_2| + \varepsilon |s|^2/2 + 2\delta_1 \|PB\| \|\tilde{x}\| \\ &\quad - [Q_m - 2\xi_1 P_M - \varepsilon P_M] \|\tilde{x}\|^2 \\ &\leq -[\gamma_1 |s|^2 + \gamma_2 |\hat{s}|] + c_1 |s|^2 + c_2 |s| \|\tilde{x}\| \\ &\quad + (c_3 + 2\delta_1 \|PB\|) \|\tilde{x}\| + c_4 |s| + c_5 \|\tilde{x}\|^2 + \varepsilon |s|^2/2 \\ &\quad - [Q_m - 2\xi_1 P_M - \varepsilon P_M] \|\tilde{x}\|^2 \\ &= -(\gamma_1 - \varepsilon/2 - c_1) |s|^2 + c_2 |s| \|\tilde{x}\| \\ &\quad - (Q_m - 2\xi_1 P_M - \varepsilon P_M - c_5) \|\tilde{x}\|^2 \\ &\quad - \gamma_2 |\hat{s}| + (c_3 + 2\delta_1 \|PB\|) \|\tilde{x}\| + c_4 \|s\|.\end{aligned} \tag{A5}$$

Using the result in (41) gives

$$\dot{\bar{V}} \leq -v^T \Gamma v, \tag{A6}$$

where $v^T = [|s| \ \ \|\tilde{x}\|]$ and Γ is described in (35). If $\gamma_1 - \varepsilon/2 - c_1 > 0$ and $|\Gamma| > 0$ then $\dot{\bar{V}} \leq 0$ (or $\dot{V} \leq -\varepsilon V$) is achieved. From (11), (12), (23) and by coordinate transformation, $\{s, \hat{s}, u, u_v, x, \hat{x}, \Psi, \hat{\Psi}\}$ are UUB. The system performance exponentially converges to the region (36).

ACKNOWLEDGEMENT

The authors would like to gratefully acknowledge the financial support provided by the National Science

Council of Taiwan, R.O.C., under grant no. NSC91-2212-E-036-006, and by Tatung University under grant no. B9208-M05-035.

REFERENCES

1. Uchino Kenji, *Ferroelectric Devices*, Marcel Dekker: Inc., New York, Basel (2000).
2. Zhang, B. and Z. Zhu, "Developing a Linear Piezomotor with Nanometer Resolution and High Stiffness," *IEEE/ASME Trans. Mechatron*., Vol. 2, No. 1, pp. 22-29 (1997).
3. Meldrum, D. R., "A Biomechatronic Fluid-Sample-Handling System for DNA Processing," *IEEE/ASME Trans. Mechatron*., Vol. 2, No. 2, pp. 99-109 (1997).
4. Choi, S. B., H. K. Kim, S. C. Lim, and Y. P. Park, "Position Tracking Control of An Optical Pick-Up Device Using Piezoceramic Actuator," *Int. J. Mechatron.*, Vol. 11, pp. 691-705 (2001).
5. Chang, T. and X. Sum, "Analysis and Control of Monolithic Piezoelectric Nano-Actuator," *IEEE Trans. Contr. Syst. Technol*., Vol. 9, No. 1, pp. 69-75 (2001).
6. Robbins, W. P., D. L. Polla, and D. E. Glumac, "High-Displacement Piezoelectric Actuator Utilizing a Meander-Line Geometry — Part I: Experimental Characterization," *IEEE Trans. Ultrason. Ferroelec. Freq. Contr*., Vol. 38, No. 5, pp. 454-460 (1991).
7. Robbins, W. P., "High-Displacement Piezoelectric Actuator Utilizing a Meander-Line Geometry — Part I: Theory," *IEEE Trans. Ultrason. Ferroelec. Freq. Contr*., Vol. 38, No. 5, pp. 461-467 (1991).
8. Song, D. and C. J. Li, "Modeling of Piezo Actuator's Nonlinear and Frequency Dependent Dynamics," *Int. J. Mechatron.*, Vol. 9, pp. 391-410 (1999).
9. Adriaens, H., W. L. de Koning, and R. Banning, "Modeling Piezoelectric Actuators," *IEEE/ASME Trans. Mechatron.*, Vol. 5, No. 4, pp. 331-341 (2000).
10. Mrad, R. B. and H. Hu, "A Model for Voltage-to-Displacement Dynamics in Piezoceramic Actuators Subject to Dynamic-Voltage Excitations," *IEEE/ASME Trans. Mechatron*., Vol. 7, No. 4, pp. 479-489 (2002).
11. Chen, B. M., T. H. Lee, C. C. Hang, Y. Guo, and S. Weerasooriya, "An H^{∞} Almost Disturbance Decoupling Robust Controller Design for a Piezoelectric Bimorph Actuator with Hysteresis," *IEEE Trans. Contr. Syst. Technol*., Vol. 7, No. 2, pp. 160-174 (1999).
12. Ge, P. and M. Jouaneh, "Tracking Control of a Piezoceramic Actuator," *IEEE Trans. Contr. Syst. Technol*., Vol. 4, No. 3, pp. 209-216 (1996).
13. Hwang, C. L., C. Jan, and Y. H. Chen, "Piezomechanics Using Intelligent Variable Structure Control," *IEEE Trans. Ind. Electron*., Vol. 48, No. 1, pp. 47-59 (2001).
14. Halim, D. and S. O. R. Moheimani, "Spatial H_2 Control of a Piezoelectric Laminate Beam: Experimental Implementation," *IEEE Trans. Contr. Syst. Technol*., Vol. 10, No. 4, pp. 533-546 (2002).
15. Utkin, V. I., "Variable Structure with Sliding Modes," *IEEE Trans. Automat. Contr*., Vol. 22, No. 2, pp. 212-222 (1977).
16. Hwang, C. L., "Design of Servocontroller via the Sliding Mode Technique," *IEE Proc.-D, Contr. Theory Appl.*, Vol. 139, No. 5, pp. 439-46 (1992).
17. Pandian, S. R., F. Takemura, Y. Hayakawa, and S. Kawamura, "Pressure Observer-Controller Design for Pneumatic Cylinder Actuators," *IEEE/ASME Trans. Mechatron*., Vol. 7, No. 4, pp. 490-499 (2002).
18. Isidori, A., *Nonlinear Control System*, Springer-Verlag, London Limited, 3rd Ed. (1995).
19. Khalil, H. K., *Nonlinear Systems*, Prentice-Hall, Inc., 2nd Ed., New Jersey (1996).

Chih-Lyang Hwang received to B.E. degree in Aeronautical Engineering from Tamkang University, Taiwan, R.O.C., in 1981, the M.E. and Ph.D. degree in Mechanical Engineering from Tatung Institute of Technology, Taiwan, R.O.C., in 1986 and 1990, respectively.

Since 1990, he has been with the Department of Mechanical Engineering of Tatung Institute of Technology, where he is engaged in teaching and research in the area of servo control and control of manufacturing systems. He received a number of awards, including the Excellent Research Paper Award from the National Science Council of Taiwan and Hsieh-Chih Industry Renaissance Association of Tatung Company. Since 1996, he is a Professor of Mechanical Engineering of Tatung Institute of Technology. In 1998-1999, he was a research scholar of George W. Woodruf School of Mechanical Engineering of Georgia Institute of Technology, USA. He is the author or coauthor of about 70 journal and conference papers in the related field. He is a technical committee of IEEE IECON02. His current research interests include fuzzy (neural-network) modeling and control, variable structure control, mechatronics, robotics, visual tracking system, and network-based control.

Chau Jan was born in Taiwan, in 1972. He received the B.E. degree from the Department of Mechanical Engineering, National Cheng Kung University, Taiwan, Taiwan, R.O.C., in 1996, and the M.E. and Ph.D. degrees in mechanical engineering from Tatung University, Taipei, Taiwan, R.O.C., in 1998 and 2003, respectively.

Since 2003, he has been with the Department of Mechanical Engineering, Nan Jeon Institute of Technology, Tainan, Taiwan, R.O.C., where he is engaged in teaching and research in the area of applied electronics and dynamic systems. His research interests include control theory, dynamic systems, electromechanics, piezomechanics robust control, neural networks, fuzzy systems.